Exploring charge transport properties and functionality of molecule-nanoparticle ensembles

Devid, E.J.

4

Enhancing the molecular signature in molecule-nanoparticle networks via inelastic cotunneling

Here, we investigate charge transport in networks of nanoparticles linked by molecular spacers, as a function of temperature. Specifically, we compare octanethiol-based structures with networks containing dithiolated OPE3. Around room temperature, the resistance ratio of these two types of devices is around 50. However, at lower temperatures, this ratio increases dramatically, to 10^5. We demonstrate that this is a result of crossing from the sequential tunneling regime to the inelastic cotunneling regime. The consequence is that the intrinsic molecular properties can be amplified through nanoscale engineering.

This chapter is based on the article published in Adv. Mater., **25**, (2013), 400-404.
Enhancing the Molecular Signature in Molecule-Nanoparticle Networks via Inelastic Cotunneling, J.-F. Dayen, E. J. Devid, M. V. Kamalakar, D. Golubev, C. M. Guédon, V. Faramarzi, B. Doudin and S. J. van der Molen.

4.1 Introduction of molecule-nanoparticle ensembles

In the field of molecular charge transport, several techniques have been developed to probe molecular conductance properties, ranging from mechanically controllable break junctions to large-area molecular junctions [1]. Two-dimensional (2D) molecule-nanoparticle ensembles have proven to combine several advantageous properties [2-4]. In these structures the gold nanoparticles are ordered in a triangular 2D-network and bridged by a molecular species of choice. In such networks the sheet resistance R is a direct measure of the (spatially averaged) conductance value of a nanoparticle-molecule-nanoparticle junction, R_T. This provides direct macroscopic access to the charge transport through molecules. Furthermore, these networks are defect-tolerant, resulting in device robustness, in particular when compared to most molecular devices. Finally, the molecules within the network are easily probed or addressed by an external stimulus, such as light. The latter provides the unique possibility to investigate the properties of these molecules that may possess a passive or active functionality. A nice example of active functional molecules are switchable light-sensitive molecules. These molecules have demonstrated their reversible photochromic switching for several types of diarylethene derivatives inserted within molecular-nanoparticle arrays [5-7]. Opto-electronic devices based on functional nano-sized elements have become possible.

The critical question remains if such devices can reach high on-off ratios (on-state conductance divided by off-state conductance), i.e. ratios of several orders of magnitude. Here, we investigate a principle path towards enhancing this ratio artificially, by making use of the electrostatic properties of the nanoparticles advantageously. Below, we present the concept in a nut shell.

From a simple perspective, molecule-nanoparticle ensembles can be described as granular systems containing metal particles, where these particles are embedded in an insulating molecular matrix [8]. However, molecule-nanoparticle ensembles will display an intricate combination of the properties of both ingredients: the molecules and the metal nanoparticles. The effect of the metal nanoparticles in a molecule-nanoparticle ensemble is the following. The smaller these nanoparticles get, the stronger the effect of local electron-electron repulsion will be. If the thermal energy is lower than the typical energy needed to move an electron to a neighbouring nanoparticle (the charging energy, E_C), the nanoparticles cannot be treated as ideal

metallic shorts any longer, and the Coulomb energy barrier suppresses transport (see Figure 4.1(a)). This is called Coulomb blockade [9]. Still, some current can flow, and at lower temperatures this happens via a process called multiple inelastic cotunneling (see below for more details). This process, illustrated in Figure 4.1(b), involves coordinated charge transfer of several charges through typically *j* junctions (where *j* can be 2, 3, 4, .,.) [8, 10-13]. As a result, the conductance of a network device will be related to the product of the transfer probabilities of each junction involved. In other words, the network's resistance will approximately scale with $(R_T)^j$, where R_T denotes the resistance of a single (molecular) junction. This differs significantly from the linear scaling of network resistance with R_T, which is expected when Coulomb blockade does not occur (see Chapter 3). The above has a remarkable consequence for networks containing switchable molecules. In the multiple cotunneling regime, the on-off ratio *P* of such devices will scale as $P = \frac{R_{device}^{OFF}}{R_{device}^{ON}} = \left(\frac{R_{mol}^{OFF}}{R_{mol}^{ON}}\right)^j$. Thus, the on-off ratio of the device is enhanced by a power $j > 1$ as compared to the on-off ratio of a single molecular junction.

Here, we present a proof-of-principle experiment of this 'enhancement' via inelastic multiple cotunneling. To do so, we use the methodology of molecular exchange in 2D nanoparticle networks. We compare two types of *passive* networks: one with a higher resistance (based on octanethiols, comparable to an 'off-state') and one with a lower resistance (the same networks, but after an OPE3-dithiol exchange step, representing the "on-state"). The procedure behind molecular exchange is explained in paragraph 3.2 and also in past reports [3, 4, 6].

Systematic temperature-dependent transport measurements on so-called nanotrench devices (see below and see paragraph 3.4) will be presented to provide a more complete insight into the regimes of conduction. Interestingly, the work described here also sheds new light on a set of recent experiments which have shown different current-voltage dependencies [14-16]. We demonstrate that these dependencies are signatures of cotunneling processes in different regimes. Indeed, the unique possibility to modify the interparticle tunneling probability via molecular exchange, allows us to provide a unified picture of conduction in ordered 2D networks. Let us first gain further insight in the regimes expected.

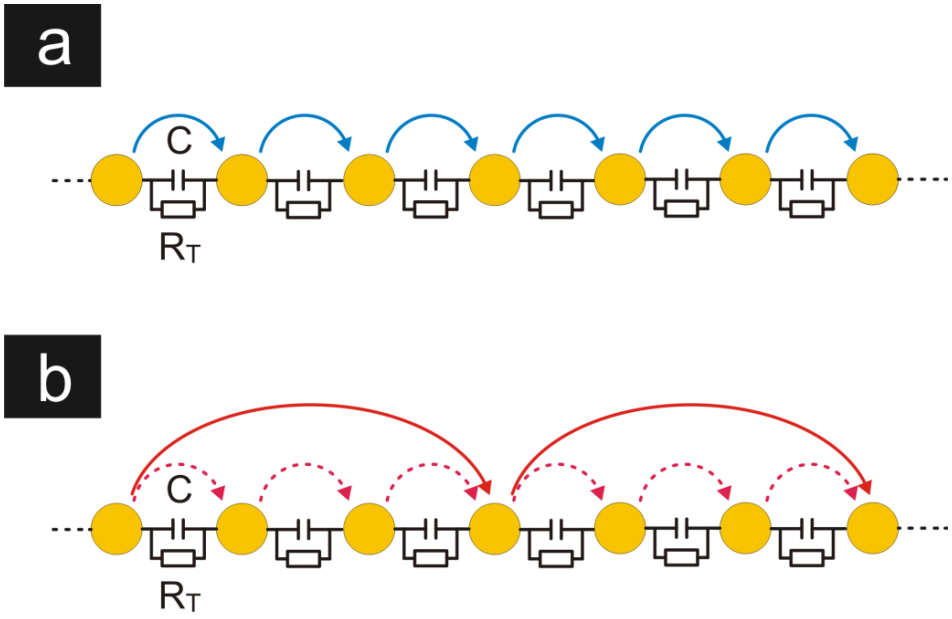

Figure 4.1: Simplified diagrams of the nanoparticle circuit, with Au clusters (yellow circles), having charging energy E_C, separated by molecular spacers of resistance R_T. (a) The sequential tunneling diagram shows tunneling between neighbours as the origin of conduction (represented by small blue solid arrows). (b) The cotunneling regime diagram illustrates how charge transfer takes place through a succession of jumps (large red solid arrows) involving cooperative tunneling of j electrons (small red dashed arrows) through $j + 1$ nanoparticles.

4.2 Charge transport mechanisms expected

Several regimes of charge transport are accessible for molecule-nanoparticle ensembles. The manifestation of these will depend on detailed characteristics, such as the molecular species used, the nanoparticle properties and the structuring of the ensemble itself [17].

Let us first consider elevated temperatures, i.e. $k_B T \gg E_c$; the regime where the nanoparticles behave as simple metal electrodes. Transport is then dominated by sequential (off-resonant) tunneling from one gold particle to another via the molecule(s) in between them. Hence, the conductance of a network is directly proportional to the conductance of the molecular intermediates (see Chapter 1 and 3). At lower temperatures, i.e. $k_B T \leq E_c$, however, transport is strongly affected by Coulomb

interaction between the electrons. If an electron tunnels from one nanoparticle to a neighbouring one, both of them become electrically charged, i.e., one with a hole, one with an electron. The electrostatic energy associated with this charge configuration for a nanoparticle, the charging energy E_C, plays a central role in theory as it raises a barrier for transport. This energy can be written as $E_C = \frac{e^2}{2C}$, where e is the electron charge and C is the total capacitance associated with a nanoparticle in a network. The latter depends on the number of nanoparticles surrounding a single nanoparticle with self-capacitance C_s. Specifically, we have $C = C_s + \sum C_i$, where, C_i is the capacitance with respect to each of the neighbouring particles. Charging effects can dramatically suppress electron transport. For a nanoparticle network exhibiting Coulomb blockade, the conductance properties can be described by the (semi-classical) 'orthodox theory', assuming the metal nanoparticles in alkanethiol-metal nanoparticle ensembles have periodic ordering [18-20]. In this regime, the sequential contribution to the conductance becomes exponentially suppressed via an Arrhenius relation:

$$G \propto e^{-E_C/k_BT}, \tag{4.1}$$

where higher order processes are ignored. Interestingly, however, in weakly coupled gold nanoparticle assemblies, the conductance values start to deviate from orthodox theory at lower temperatures [14, 16, 18, 21]. In fact, (multiple) inelastic cotunneling becomes important. In this regime, a set of virtual states allow for cooperative electron transfer over length scales beyond one particle-particle distance, leaving a hole behind (see Figure 4.1(b)) [14].

Unfortunately, a quantitative analysis of multiple inelastic cotunneling transport in granular metals is very difficult, because of the complexity of the exact analytical expressions for the current. In order to overcome this problem, Belobodorov *et al.* [14] have proposed an approximate formula which captures the basic physics. For an ideal system with identical tunnel (or in our case: molecular) resistances and equal charging energy for all nanoparticles, a model reminiscent to variable range hopping, referred to as variable range cotunneling (VRC), yields a current I versus voltage V relation given by [14]:

$$I \propto V_{jct} \sum_j \left(\frac{h}{e^2 R_T}\right)^j \left(\frac{{k_B}^2 T^2 + e^2 {V_{jct}}^2}{{E_C}^2}\right)^{j-1} exp\left(-\frac{\frac{E_C}{j} - jeV_{jct}}{k_B T}\right). \tag{4.2}$$

The current in this model is given by a Taylor series in the small parameter h/e^2R_T . Here T is the temperature, k_B Boltzmann's constant, and $V_{jct} = V/N$ is the voltage drop over a single tunnel junction connecting two neighbour nanoparticles (with N the total number of tunnel barriers along the array). The summation in equation 4.2 runs over the number of junctions j involved in the cotunneling events.

To appreciate equation 4.2, we first note that the contribution of cotunneling through j junctions is proportional to $(h/e^2R_T)^j$ and hence decreases strongly with increasing j. Still, at lower temperatures, multiple cotunneling may become the dominant process. This is due to a counterbalancing effect, which is related to the Boltzmann term in equation 4.2. In fact, the electrostatic potential barrier associated with the process decreases with increasing j. The reason for this is that an electron and a hole created in the array after a cotunneling event are separated by j junctions. In the experimentally relevant case of weak screening, one can roughly estimate the interaction energy between them as $U \sim e^2/\varepsilon L$, where L is the distance between the nanoparticles hosting the electron and the hole. Since $L = jr$ in closely packed array of particles, with r the average center-to-center distance between two nanoparticles, this energy U may be transformed to a form that explicitly reveals the reduction of the potential barrier: $U \approx E_C / j$.

All in all, the competition between the decreasing factor $(h/e^2R_T)^j$ and increasing activation exponent $e^{(-U/k_BT)}$ with j, determines the optimal number of junctions, $j_{opt} \equiv N_{cot}$, through which cotunneling occurs. At low temperatures, N_{cot} may reach 5 or even more. To illustrate this, Figure 4.2 shows an example calculation of the current's dependence on temperature and j via cotunneling, according to equation 4.2.

Figure 4.2(a) displays how the partial current, associated with each (co)tunnel process involving j junctions, increases with temperature. (Note that the total current versus temperature is given by the sum of these curves, for all j.) Clearly, the current due to sequential tunneling ($j = 1$) dominates at higher temperatures. However, as T decreases, a transition occurs to multiple cotunneling. First, the current due to $j = 2$ dominates, so here $N_{cot} = j_{opt} = 2$. At even lower T, higher values of N_{cot} can be found. Figure 4.2(b) displays the same data set in a different plot, showing partial current values for a series of temperatures versus j. Here, the competition between the cotunneling probability factor $(h/e^2R_T)^j$ and the activation term $e^{(-E_c/jk_BT)}$ is visualized more clearly.

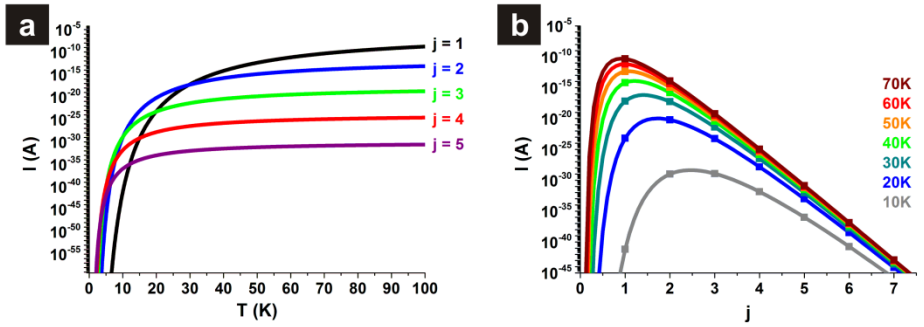

Figure 4.2: (a) Calculation of the partial current for each of the (multiple co-)tunneling processes, involving j junctions, as a function of temperature. (b) Partial current versus j at various temperatures. Both (a) and (b) are calculated from equation 4.2, using R_T = 1 MΩ, V_{jct} = 0.5 mV, E_C = 0.072 eV.

Again, we see that at lower temperatures the optimal $j_{opt} = N_{cot}$ shifts to values greater than 1. In Appendix A.1, we derive the approximate temperature-dependence of N_{cot} to find:

$$N_{cot} \approx \sqrt{\frac{E_C}{k_B T \ln(e^2 R_T/h)}} \propto 1/\sqrt{T}. \qquad (4.3)$$

Finally, we note that the summation in equation 4.2 is restricted by the requirement of a positive potential barrier, $U > 0$. This specifically has consequences for the case of high applied biases. Since the effective voltage drop over the set of j junctions lowers the Boltzmann term, the requirement $U > 0$ restricts the number of junctions to: $j \leq N_{max} \approx \sqrt{E_C/eV_{jct}}$. Formally, higher values of j also contribute to the current, but the corresponding terms do not contain an activation exponent. Since this eliminates the term favouring higher j, the full expression quickly decays with increasing j. Thus these terms can be ignored.

At low temperatures, when the charging energy E_C becomes larger than $k_B T$, equation 4.2 predicts how the current will evolve with voltage-bias. Interestingly, this relation can be approximated by three asymptotic expressions (see Appendix A.1), categorized as cotunneling regimes C1, C2, and C3, for different voltage ranges between neighbouring particles:

C1: $I \propto V$, for $eV_{jct} \ll k_B T$. (4.4)

C2: $I \propto V^{\alpha}$, where $\alpha = 2N_{cot} - 1$, for $k_B T < eV_{jct} < k_B T \ln\left(\frac{e^2 R_T}{h}\right)$. (4.5)

C3: $I \propto \exp\left[-\sqrt{\frac{V^*}{V}}\right]$, for $k_B T \ln\left(\frac{e^2}{h} R_T\right) < eV_{jct}$. (4.6)

In regime C1, i.e. the very low-bias regime, equation 4.2 yields Ohmic behaviour.

In regime C2, the middle part of equation 4.2, which stems directly from cotunneling theory, becomes important. This results in a strong power law dependence of the $I(V)$ curves, with a power that depends on N_{cot}.

Finally, an interesting regime is reached in C3, where the current scales with voltage in an Efros-Shklovskii-like fashion, but with temperature replaced by voltage. In other words, the current depends exponentially on $-\sqrt{V^*/V}$, where V^* is a constant related to E_C and R_T. Interestingly, this relation connects to the temperature-dependence expected for low-bias voltages (within regime C1). In that situation, a true Efros-Shklovskii dependence is anticipated, i.e.

$$G \propto \exp\left[-\sqrt{\frac{T^*}{T}}\right], \quad (4.7)$$

where T^* depends on E_C and R_T and is approximately constant (see Appendix A.1).

For completeness, at very high voltage biases $eV_{jct} \approx E_C$, the system is in the sequential tunneling regime, as first proposed by Ref. [22].

4.3 Charge transport measurements on nanotrench devices

To fully characterize transport mechanisms, temperature and bias voltage are to be varied over a wide range. Anticipating the sample resistance to dramatically increase when lowering the temperature, a device structure (called a nanotrench device, see paragraph 3.4) with a large width-to-length aspect ratio (~100) is used. This limits the number of nanoparticles spanning the gap between the electrodes. In this way, our samples, involving a minimum number of charge transfer steps, avoid percolation or distributions of cotunneling domain sizes which often complicate the data interpretation. Furthermore, we make use of the advantageous possibility to modify the inter-particle resistance values in the molecule-gold nanoparticle network by molecular exchange. This gives us an extra tool to assess conduction.

For the nanotrench devices, electron beam lithography is used to pattern Ti (3 nm)/Au (47 nm) electrodes separated by a gap of 100-150 nm length and 10 μm width over silicon oxide substrate. On top of these structures, a two-dimensional network of coated gold nanoparticles (~8.5 nm in diameter, covered with octanemonothiols: "C8") is deposited using a polydimethylsiloxane (PDMS) microcontact printing method, following literature procedures [3, 4, 6, 23, 24]. Unlike stamping large arrays between widely gapped electrode pairs, [3, 4, 6, 7, 25, 26] the process of stamping between narrowly spaced electrodes proved quite challenging and order is only locally conserved. A typical sample can be seen in Figure 4.3.

We first characterized the as-prepared samples, with C8 spacers, at room temperature. Low-temperature electrical measurements were carried out using a semiconductor parameter analyzer suitable for low-signal measurements, with samples inside a He-flow cryostat of 1.5 K base temperature. Figure 4.4(a) shows temperature-dependent *I-V* curves for a typical C8 sample. After characterization, the C8 samples were transferred to a glove box, where a molecular exchange procedure with conjugated oligo(phenylene ethynylene)-dithiol (OPE) molecular bridges (referred as OPE state) was performed, in an OPE solution in tetrahydrofuran for 24 hours. This resulted in a decrease of the room-temperature resistance of typically two orders of magnitude, in agreement with previous reports [3, 26]. The OPE-samples were then studied as a function of temperature.

We found good reproducibility after temperature sweeps (without hysteresis), confirming the robustness of our samples. We also checked that molecular exchange was reversible, by confirming that the temperature-dependent transport of a C8 back-exchanged sample was similar to the initial C8 sample. Finally, measurements were reproducible from sample to sample, within a scaling factor related to the nanotrench filling after stamping the particles.

4.4 Charge transport properties of C8 and OPE exchanged gold nanoparticle networks

Measurements of *I-V* curves for various temperatures are presented in Figures 4.4(a) and 4.4(b), for C8 and OPE (i.e. exchanged) samples, respectively. All samples showed a transition from ohmic behaviour at room temperature, to non-linear behaviour below a temperature in the 100 K to 200 K range.

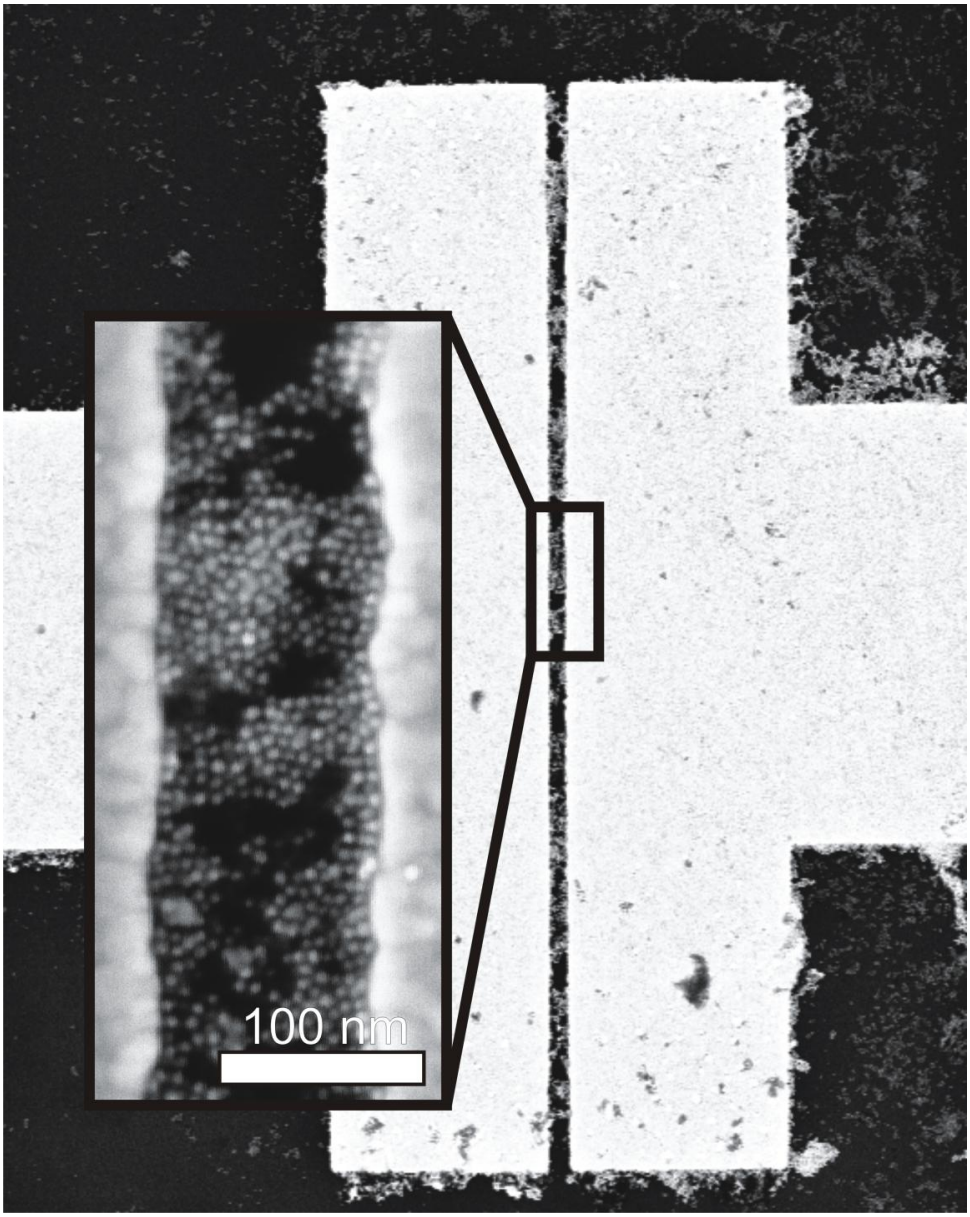

Figure 4.3: Scanning electron microscope image of a 2D nanoparticle network sample with a zoomed inset showing the nanotrench coverage.

In the same temperature range the low-bias resistance also increases significantly (see inset of Figure A-1(a) in Appendix A.2). This is consistent with the charging energy of the nanoparticles estimated from the simplest two concentric shells model,

$$E_C = \frac{e^2}{8\pi\varepsilon_0\varepsilon_r}\left(\frac{1}{r} - \frac{1}{r+d}\right), \tag{4.8}$$

with ε_0 the vacuum permittivity, ε_r the relative permittivity of the molecules surrounding the nanoparticles of radius r and separation d. This gives $E_C^{C8} \approx 17$ meV $\simeq$ 200 K and $E_C^{OPE} \approx 14$ meV $\simeq$ 150 K, respectively. The slight change of charging energy when exchanging the molecules, interpreted as a modification of the medium permittivity, is consistent with our findings of the C8 state having a slightly more pronounced non-linear behaviour at low temperatures, which can be interpreted as an increase of the charging energy, not exceeding twice the OPE value.

Power-law behaviour of the *I-V* curves is illustrated in Figure 4.4(c), where the data for an OPE sample are plotted double-logarithmically. At sufficiently high temperatures, i.e. when the thermal energy overcomes the charging energy E_C, the network exhibits an almost ohmic behaviour, with a macroscopic sheet resistance proportional to R_T. At lower temperatures, but at high-bias voltages, $eV_{jct} \sim E_C$, sequential tunneling through the blockaded islands becomes the dominant process. The corresponding region is indicated as "sequential" (labelled "seq" in Figure 4.4(c)). This regime has been discussed in much detail in literature [17, 22, 27]. At low biases and low temperatures, however, the VRC regime is entered, described by equation 4.2, which is at the heart of this study. Figure 4.4(c) separates the areas where regimes C1, C2 and C3 apply (see equation 4.4 till 4.6 and Appendices A.3 and A.4). Within region C1, linear *I-V* curves are found (see equation 4.4). In contrast, in the C2 zone indicated, the slope on the double-logarithmic scale reveals power-law behaviour with an exponent that depends on temperature, reaching values of up to 7 (see equation 4.5). Indeed, Tran *et al.* also reported temperature-dependent power law behaviour, characteristic of the regime C2, with similar exponents [14, 15].

On the other hand, Moreira *et al.* recently emphasized the applicability of an Efros-Shklovskii-type relation, comparable to equation 4.6. They explained this behaviour phenomenologically, by assuming that the voltage dependence for cotunneling mirrors the zero-bias temperature dependence [11, 12].

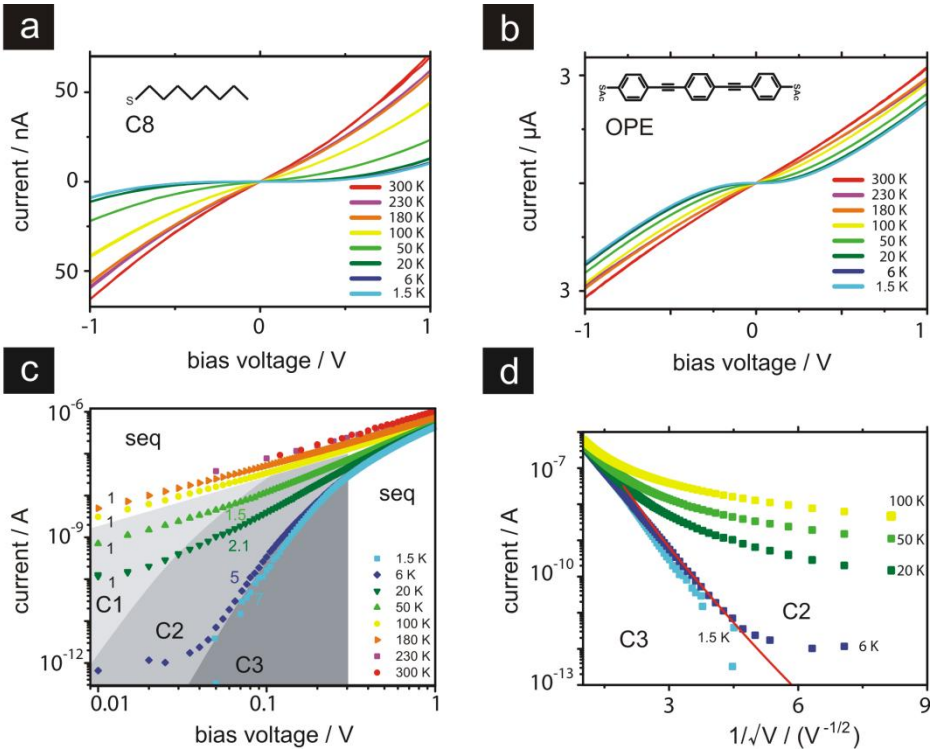

Figure 4.4: *I-V* curves of a nanoparticle network, in the C8 (Figure 4.4(a)) and OPE (Figure 4.4(b)) states respectively, measured at several temperatures. (c) Log-Log plot of OPE data, illustrating the power law behaviour, $\boldsymbol{I \propto V^{\alpha}}$, and discriminating the different conductance regimes (data are taken from a second sample). $\alpha = 1$ is expected in the sequential tunneling (labelled "seq") and thermally activated cotunneling (labelled "C1") regimes. In regime C2 (multiple inelastic cotunneling), however, the number of cotunneling events, N_{cot}, relates to $\alpha = 2N_{cot} - 1$ (with an exponent between 1.5 and 7, indicated next to the curves). (d) Semilog plot of current versus $1/\sqrt{V}$ for the data set in Figure 4.4(c), illustrating the transition between regime C2 and the Efros-Shklovskii-like behaviour (regime C3), observed at the lowest temperatures. See Appendix A.3 for a similar analysis of the $I(V)$-curves in panels (a)-(b).

Our experimental results (see Figures 4.4(c) and 4.4(d)), show that the lowest-temperature *I-V* curves turn out to be at the boundary between the power law form (region C2) and Efros-Shklovskii-type voltage dependence (region C3).

The distinction between the power law behaviour of regime C2 and the Efros-Shklovskii-type behaviour of regime C3, however, is not visible on a log-log plot such as Figure 4.4(c) due to the limited *V* and *I* ranges. In order to check the existence of regime C3 at high-bias and low temperature, we replot the data in an Efros-type plot with voltage playing the role of temperature, i.e., we plot the current semi-logarithmically versus $1/\sqrt{V}$. In addition, for full consistency, the transition from C2 to C3 regimes should take place close to the C2-C3 delimitation line predicted by the theory. In Figure 4.4(d) we illustrate that the lowest-temperature curves also satisfy a $I \propto exp\left(-\sqrt{V^*/V}\right)$ dependence, expected for regime C3 (see equation 4.6). Moreover, as it can be seen in Figure 4.4(c) and 4.4(d), the region at which the transition from C2 to C3 is observed, matches well with the boundary predicted by theory (see also Appendix A.4). In Appendix A.3, we show that the same observations and conclusions hold for the C8 case. Our measurements therefore indicate that the discrepancy between transport regimes reported previously (power law versus Efros-Shklovskii-like) [14-16] can possibly be explained within a model of multiple inelastic cotunneling based on the equation 4.2. The transfer between the various regimes is continuous. This is the first main conclusion of this work.

Interestingly, the cotunneling regime corresponds to a charge transfer probability proportional to $(R_T)^{N_{cot}}$ i.e. the product of the resistances of the N_{cot} junctions involved. This specific property leads to new opportunities for device applications, especially when seeking for increased susceptibilities. Spin-dependent resistance in magnetic systems enhanced by cotunneling is a well-documented example [28], as recently shown in a nanoparticles network [13]. Figure 4.5 provides a more complete insight into the transport properties in regime C2. To show that the deduced N_{cot} values are robust, the temperature-dependent N_{cot} values are plotted as a function of $\sqrt{1/T}$ (see Figure 4.5(a)), as anticipated by equation 4.3. The N_{cot} values are deduced from fitting the *I-V* curves in the C2 region to the power law $I \propto V^{2N_{cot}-1}$ for several samples, both in the C8 and OPE states (see also Appendices A.3 and A.4). The change of R_T when exchanging the molecules does not significantly alter the number of particles over which coherent cotunneling occurs, here taking place over 1 to 4 particles when cooling down the samples. Having gained confidence that the data of C8 and OPE

relate to similar numbers of cotunneling events, the evolution of the current scales ratio between the two type of molecules when cooling down can be made explicit.

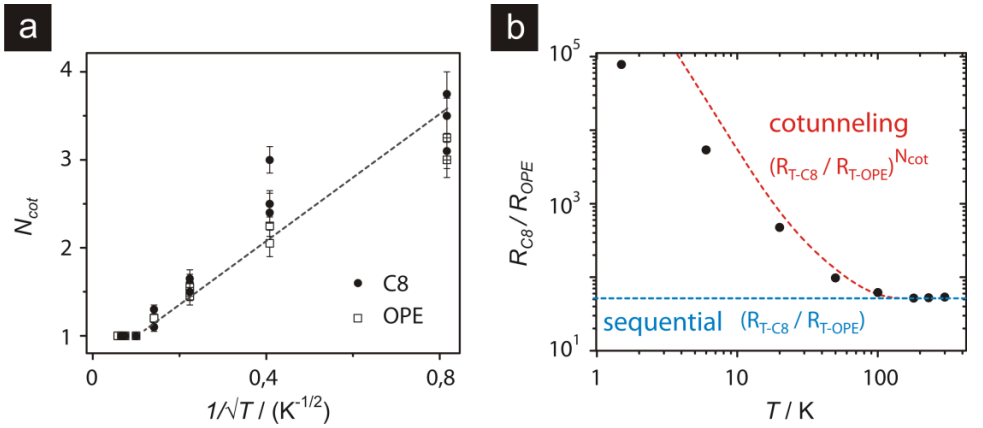

Figure 4.5: (a) The number of junctions N_{cot} involved in a cotunneling event at several temperatures, for several samples in C8 and OPE states. The dotted line is a guide to the eye, following the model of inelastic multiple cotunneling $N_{cot} \approx \sqrt{E_C / k_B T \, ln(e^2 R_{jct}/h)}$. (b) The temperature evolution of the resistance ratio R_{C8}/R_{OPE} of the network resistance in the C8 and OPE states. The red dotted line shows the model behaviour, with a transition from classical regime $R_{C8}/R_{OPE} \propto R_{T-C8}/R_{T-OPE}$, to cotunneling regime $R_{C8}/R_{OPE} \propto (R_{T-C8}/R_{T-OPE})^{N_{cot}}$. The blue dotted line shows the expected curve for sequential tunneling only.

The key experimental outcome, demonstrating enhanced susceptibility, is shown in Figure 4.5(b). The ratio R_{C8}/R_{OPE}, i.e. the ratio of the full network resistances before and after molecular exchange, is around 50 at room temperature, and it remains unchanged down to 200 K, i.e. as long as the samples are in the sequential tunneling regime. At lower temperatures, however, the sample enters the cotunneling regime and this ratio increases up to 10^5, now being governed by $(R_{T\text{-}C8}/R_{T\text{-}OPE})^3$ to $(R_{T\text{-}C8}/R_{T\text{-}OPE})^4$ at 1.6 K (cf. Figure 4.5(a)). This spectacular increase of R_{C8}/R_{OPE} ratio matches well with the cotunneling trend expected (see red dotted line in Figure 4.5(b). These results are hence a direct indication of cotunneling processes taking place in nanoparticles network.

4.5 Conclusions

In conclusion, molecular exchange in metallic nanoparticle-molecule networks is a high-value tool for validating a complete picture of cotunneling. By putting our data in the light of equation 4.2, a simple picture of cotunneling transport signatures related to the probed energy scale allows us to reconcile the different approaches found in the literature. The temperature change of the number N_{cot} of junctions involved in cotunneling confirms the trend $N_{cot} \propto \sqrt{1/T}$, as expected from a variable range cotunneling model.

Additionally, we show that in the cotunneling regime a resistance modification can be amplified by several orders of magnitude. This enhancement is also expected for systems for which molecular transport properties are modified under external conditions. For example, the on/off ratio of light-sensitive switchable molecular devices may be strongly improved in this way. To utilize this effect at room temperature, networks based on smaller nanoparticles (roughly < 5 nm in diameter) should be used. All in all, nanoparticle-based molecular devices do not only have advantages in terms of robustness and reproducibility, but also in terms of enhanced susceptibility to external stimuli. The future expectation is that these nanoparticle-based molecular devices can be of valuable use to a wide variety of multifunctional molecular materials.

4.6 References

1. H. B. Akkerman, P. W. M. Blom, D. M. de Leeuw and B. de Boer, Electron Tunneling Through Alkanedithiol Self-assembled Monolayers in Large-area Molecular Junctions, *Nature*, **441**, (2006), 69-72.
2. R. P. Andres, J. D. Bielefeld, J. I. Henderson, D. B. Janes, V. R. Kolagunta, C. P. Kubiak, W. J. Mahoney and R. G. Osifchin, Self-assembly of a Two-dimensional Superlattice of Molecularly Linked Metal Clusters, *Science*, **273**, (1996), 1690-1693.
3. J. Liao, L. Bernard, M. Langer, C. Schönenberger and M. Calame, Reversible Formation of Molecular Junctions in 2D Nanoparticle Arrays, *Adv. Mater.*, **18**, (2006), 2444-2447.
4. L. Bernard, Y. Kamdzhilov, M. Calame, S. J. van der Molen, J. Liao and C. Schönenberger, Spectroscopy of Molecular Junction Networks Obtained by Place Exchange in 2D Nanoparticle Arrays, *J. Phys. Chem. C*, **111**, (2007), 18445-18450.

5. K. Matsuda, H. Yamaguchi, T. Sakano, M. Ikeda, N. Tanifuji and M. Irie, Conductance Photoswitching of Diarylethene-Gold Nanoparticle Network Induced by Photochromic Reaction, *J. Phys. Chem. C*, **112**, (2008), 17005-17010.
6. S. J. van der Molen, J. Liao, T. Kudernac, J. S. Agustsson, L. Bernard, M. Calame, B. J. van Wees, B. L. Feringa and C. Schönenberger, Light-controlled Conductance Switching of Ordered Metal-Molecule-Metal Devices, *Nano Lett*., **9**, (2009), 76-80.
7. S. J. van der Molen and P. Liljeroth, Charge Transport Through Molecular Switches, *J. Phys.: Condens. Matter*, **22**, (2010), 133001(1-30).
8. I. S. Beloborodov, K. B. Efetov, A. V. Lopatin and V. M. Vinokur, Granular Electronic Systems, *Reviews of Modern Physics*, **79**, (2007), 469-518.
9. C. J. Gorter, A Possible Explanation of the Increase of the Electrical Resistance of Thin Metal Films at Low Temperatures and Small Field Strengths, *Physica*, **17**, (1951), 777-780.
10. D. V. Averin and Y. V. Nazarov, Virtual Electron Diffusion during Quantum Tunneling of the Electric Charge, *Phys. Rev. Lett*., **65**, (1990), 2446-2449.
11. I. S. Beloborodov, A. V. Lopatin, and V. M. Vinokur, Coulomb Effects and Hopping Transport in Granular Metals, *Phys. Rev. B*, **72**, (2005), 125121(1-20).
12. M. V. Feigel'man and A. S. Ioselevich, Variable Range Cotunneling and Conductivity of a Granular Metal, *JETP Lett*., **81**, (2005), 277-283.
13. M. Pauly, J.-F. Dayen, D. Golubev, J.-B. Beaufrand, B. P. Pichon, B. Doudin and S. Bégin-Colin, Co-tunneling Enhancement of the Electrical Response of Nanoparticle Networks, *Small*, **8**, (2012), 108-115.
14. T. B. Tran, I. S. Beloborodov, J. Hu, X. M. Lin, T. F. Rosenbaum and H. M. Jaeger, Sequential Tunneling and Inelastic Cotunneling in Nanoparticle Arrays, *Physical Review B*, **78**, (2008), 075437(1-9).
15. T. B. Tran, I. S. Beloborodov, X. M. Lin, T. P. Bigioni, V. M. Vinokur and H. M. Jaeger, Multiple Cotunneling in Large Quantum Dot Arrays, *Phys. Rev. Lett.*, **95**, (2005), 076806(1-4).
16. H. Moreira, Q. Yu, B. Nadal, B. Bresson, M. Rosticher, N. Lequeux, A. Zimmers and H. Aubin, Electron Cotunneling Transport in Gold Nanocrystal Arrays, *Phys Rev Lett.*, **107**, (2011), 176803(1-5).
17. A. Zabet-Khosousi and A.-A. Dhiran, Charge Transport in Nanoparticle Assemblies, *Chemical Reviews*, **108**, (2008), 4072-4124.
18. G.-L. Ingold and Y. V. Nazarov, *Charge Tunneling Rates in Ultrasmall Junctions*. In Single Charge Tunneling; H. Grabert, M. H. Devoret, Eds.; Plenum: New York, **1992**; 21-107.
19. M. Amman, R. Wilkins, E. Ben-Jacob, P. D. Maker and R. C. Jaklevic, Analytic Solution for the Current-Voltage Characteristic of Two Mesoscopic Tunnel Junctions Coupled Ion Series, *Phys. Rev. B*, **43**, (1991), 1146-1149.
20. P. D. Dresselhaus, L. Ji, S. Han, K. Lin, J. Lukens and K. K. Likharev, Single Electron Tunneling in Single Junctions and Multi-junction Systems, Physica B: *Physics of Condensed Matter*, **194**, (1994), 1335-1336.
21. M. M. A. Yajadda, K.-H. Müller and K. Ostrikov, Effect of Coulomb Blockade, Gold Resistance, and Thermal Expansion on the Electrical Resistance of Ultrathin Gold Films, *Physical Review B*, **84**, (2011), 235431(1-8).

22. A. A. Middleton and N. S. Wingreen, Collective Transport in Arrays of Small Metallic Dots, *Physical Review letters*, **71**, (1993), 3198-3201.
23. V. Santhanam and R. P. Andres, Microcontact Printing of Uniform Nanoparticle Arrays, *Nano Lett.*, **4**, (2004), 41-44.
24. V. Santhanam, J. Liu, R. Agarwal and R. P. Andres, Self-assembly of Uniform Monolayer Arrays of Nanoparticles, *Langmuir*, **19**, (2003), 7881-7887.
25. J.-F. Dayen, V. Faramarzi, M. Pauly, N. T. Kemp, M. Barbero, B. P. Pichon, H. Majjad, S. Begin-Colin and B. Doudin, Nanotrench for Nano and Microparticle Electrical Interconnects, Nanotechnology, **21**, (2010), 335303(1-7).
26. C. M. Guédon, J. Zonneveld, H. Valkenier, J. C. Hummelen and S. J. van der Molen, Controlling the Interparticle Distance in a 2D Molecule-nanoparticle Network, *Nanotechnology*, **22**, (2011), 125205(1-5).
27. D. V. Talapin, J-S. Lee, M. V. Kovalenko and E. V. Shevchenko, Prospects of Colloidal Nanocrystals for Electronic and Optoelectronic Applications, *Chem. Rev*., **110**, (2010), 389-458.
28. K. Yakushiji, S. Mitani, F. Ernult, K. Takanashi and H. Fujimori, Spin-dependent Tunneling and Coulomb Blockade in Ferromagnetic Nanoparticles, *Phys. Rep.*, **451**, (2007), 1-35.